J|A|C|S ARTICLES

Published on Web 02/01/2010

Crystal Structure, Diffusion Path, and Oxygen Permeability of a Pr_2NiO_4-Based Mixed Conductor $(Pr_{0.9}La_{0.1})_2(Ni_{0.74}Cu_{0.21}Ga_{0.05})O_{4+\delta}$

Masatomo Yashima,*,† Nuansaeng Sirikanda,‡ and Tatsumi Ishihara‡

Department of Materials Science and Engineering, Interdisciplinary Graduate School of Science and Engineering, Tokyo Institute of Technology, Nagatsuta-cho 4259, Midori-Ku, Yokohama, Kanagawa 226-8502, Japan, and Department of Applied Chemistry, Faculty of Engineering, Kyushu University, Motooka 744, Nishi-Ku, Fukuoka, Fukuoka 819-0395, Japan

Received November 19, 2009; E-mail: yashima@materia.titech.ac.jp

Abstract: We have investigated *in situ* the crystal structure, oxygen diffusion path, oxygen permeation rate, and electrical conductivity of a doped praseodymium nickel oxide, Pr_2NiO_4-based mixed conductor, $(Pr_{0.9}La_{0.1})_2(Ni_{0.74}Cu_{0.21}Ga_{0.05})O_{4+\delta}$ (PLNCG) in air between 27 °C and 1015.6 °C. The PLNCG has a tetragonal *I*4/*mmm* K_2NiF_4-type structure which consists of a $(Pr_{0.9}La_{0.1})(Ni_{0.74}Cu_{0.21}Ga_{0.05})O_3$ perovskite unit and a $(Pr_{0.9}La_{0.1})O$ rock salt unit in the whole temperature range. Both experimental and theoretical electron density maps indicated two-dimensional networks of $(Ni_{0.74}Cu_{0.21}Ga_{0.05})$-O covalent bonds in PLNCG. Highest occupied molecular orbitals (HOMO) in PLNCG demonstrate that the electron−hole conduction occurs via Ni and Cu atoms in the $(Ni_{0.74}Cu_{0.21}Ga_{0.05})$-O layer. The bulk oxygen permeation rate was high (137 μmol cm^{-2} min^{-1} at 1000 °C), and its activation energy was low (51 kJ mol^{-1} at 950 °C). The Rietveld method, maximum-entropy method (MEM), and MEM-based pattern fitting analyses of neutron and synchrotron diffraction data indicate a large anisotropic thermal motion of the apical O2 oxygen at the 4*e* site (0, 0, *z*; $z \approx 0.2$) in the $(Pr_{0.9}La_{0.1})(Ni_{0.74}Cu_{0.21}Ga_{0.05})O_3$ perovskite unit. Neutron and synchrotron diffraction data and theoretical structural optimization show the interstitial oxygen (O3) atom at (*x*, 0, *z*) ($x \approx 0.6$ and $z \approx 0.2$). The nuclear density analysis indicates that the bulk oxide-ion diffusion, which is responsible for the high oxygen permeation rate, occurs through the interstitial O3 and anisotropic apical O2 sites. The nuclear density at the bottleneck on the oxygen diffusion path increases with temperature and with the oxygen permeation rate. The activation energy from the nuclear density at the bottleneck decreases with temperature, which is consistent with the decrease of the activation energy from oxygen permeation rate. The extremely low activation energy (12 kJ mol^{-1} at 900 °C) from the nuclear density at the bottleneck indicates possible higher bulk oxygen permeation rates in quality single crystals and epitaxial thin films.

Introduction

Mixed oxide ionic and electronic conducting ceramics (MIECs) will become increasingly important for future environmentally friendly ("green") societies because the MIECs are used as materials for oxygen separation membranes and cathodes of solid-oxide fuel cells (SOFCs).[1−4] Oxygen is an important reactant in the industrial chemical processes, and air is usually utilized as the oxygen source due to the cost problem. In comparison with air, pure oxygen is more efficient for the chemical processes, and thus, the oxygen separation from air by the permeation of oxygen through MIECs is attractive.[3−13] Oxygen can permeate through MIECs membranes when a gradient of oxygen chemical potential exists. In the ion transport membranes-oxygen systems, simultaneous conduction of ions and electrons in the same material does not require an external electrical circuit to provide the driving force for the separation, with a significant reduction in cost.[14]

Fuel cells directly and efficiently convert chemical energy to electrical energy. Of various fuel cells, the SOFCs have benefits of environmentally benign power generation with fuel flexibility. The operating temperature of SOFCs is high

† Tokyo Institute of Technology.
‡ Kyushu University.

(1) Atkinson, A.; Barnett, S.; Gorte, R. J.; Irvine, J. T. S.; Mcevoy, A. J.; Mogensen, M.; Singhal, S. C.; Vohs, J. *Nat. Mater.* **2004**, *3*, 17–27.
(2) ten Elshof, J. E.; Bouwmeester, H. J. M.; Verweij, H. *Appl. Catal., A* **1995**, *130*, 195–212.
(3) Balachandran, U.; Dusek, J. T.; Mieville, R. L.; Poeppel, R. B.; Kleefisch, M. S.; Pei, S.; Kobylinski, T. P.; Udovich, C. A.; Bose, A. C. *Appl. Catal., A* **1995**, *133*, 19–29.
(4) Tsai, C. Y.; Dixon, A. G.; Moser, W. R.; Ma, Y. H. *AIChE J.* **1997**, *43*, 2741–2750.
(5) Hundley, M. F.; Kwok, R. S.; Cheong, S. W.; Thompson, J. D.; Fisk, Z. *Physica C* **1991**, *172*, 455–464.
(6) Kharton, V. V.; Viskup, A. P.; Kovalevsky, A. V.; Naumovich, E. N.; Marques, F. M. B. *Solid State Ionics* **2001**, *143*, 337–353.
(7) Kato, S.; Ogasawara, M.; Sugai, M.; Nakata, S. *Solid State Ionics* **2002**, *149*, 53–57.
(8) Manthiram, A.; Prado, F.; Armstrong, T. *Solid State Ionics* **2002**, *152−153*, 647–655.
(9) Li, C.; Hu, T. H.; Zhang, H.; Chen, Y.; Jin, J.; Yang, N. R. *J. Membr. Sci.* **2003**, *226*, 1–7.
(10) Kharton, V. V.; Tsipis, E. V.; Yaremchenko, A. A.; Frade, J. R. *Solid State Ionics* **2004**, *166*, 327–337.
(11) Miyoshi, S.; Furuno, T.; Sangoanruang, O.; Matsumoto, H.; Ishihara, T. *J. Electrochem. Soc.* **2007**, *154*, B57–B62.
(12) Ishihara, T.; Miyoshi, S.; Furuno, T.; Sangoanruang, O.; Matsumoto, H. *Solid State Ionics* **2006**, *177*, 3087–3091.
(13) Miyoshi, S.; Furuno, T.; Matsumoto, H.; Ishihara, T. *Solid State Ionics* **2006**, *177*, 2269–2273.
(14) Drioli, E.; Romano, M. *Ind. Eng. Chem. Res.* **2001**, *40*, 1277–1300.

(800−1000 °C); thus, costs and materials compatibility are problems. The present SOFCs technology is based on cathodes, electrolytes, anodes, and interconnectors. The MIECs cathodes for SOFCs have received considerable attention because this component contributes significantly to the overall cell resistance.[15] The performance of SOFCs cathode can be significantly improved by incorporating MIECs. Bulk transport of oxygen atoms in MIECs cathode is an important process of reactions in SOFCs. The cathode materials also require a significant level of electronic conductivity.

For the cathodes and oxygen-separation membranes, the $ABO_{3-\delta}$ perovskite-type structured MIECs such as (Ln,*A*)(Co,Fe)$O_{3-\delta}$ (*A* = Sr, Ba and Ca; Ln = lanthanoid), and (Ln,Sr)(Ga,Fe)$O_{3-\delta}$, have been utilized, where the *A* and *B* are the larger and smaller cations, respectively, and δ is the concentration of oxygen deficiency.[15−19] For lower temperature devices, novel MIECs with a higher oxygen permeation rate are required. A_2BO_4-based oxides with K_2NiF_4-type structure have extensively been studied as new MIECs,[5−13,20−29] where *A* and *B* are the larger and smaller cations, respectively. We found that the oxygen permeability is considerably increased by the addition of Ga into $Pr_2(Ni_{0.75}Cu_{0.25})O_{4+\delta}$ where the δ is the concentration of excess oxygen.[20] In the previous work,[22] we reported the diffusional pathway of oxide ions in a K_2NiF_4-type mixed conductor $(Pr_{0.9}La_{0.1})_2(Ni_{0.74}Cu_{0.21}Ga_{0.05})O_{4+\delta}$ (PLNCG). We chose this chemical composition because it exhibits a high oxygen permeation rate as described in this work. Doping of La atoms at the Pr site improves the phase stability at high temperatures where the decomposition into $Pr_4Ni_3O_{10}$- and Pr_2O_3-based phases[25] does not occur, as shown in this work. Although we visualized the oxygen diffusion path of PLNCG at 1015.6 °C,[22] the structural origin of the high permeation rate of this material has not yet been established. In the present work, we report the temperature dependence of oxygen permeation rate, electrical conductivity, crystal structure, and diffusional pathway of oxide ions of the PLNCG in order to establish the structure−property relationship. The present results suggest that the doping of Ga^{3+} at the Ni^{2+} site yields a larger amount of excess oxygen around an interstitial site, which leads to greater oxygen permeability.

Experimental Section

Sample Preparation and Characterization. $(Pr_{0.9}La_{0.1})_2(Ni_{0.74}Cu_{0.21}Ga_{0.05})O_{4+\delta}$ (PLNCG) samples were prepared by a conventional solid-state reaction method. The appropriate amounts of nickel acetate and nitrates of the other constituent cations were dissolved into distilled water, followed by heating to dryness. The resultant product was pulverized with an alumina mortar and pestle, and then calcined at 800 °C for 6 h. After mixing again, the powder was pressed into disks of 20 mm in diameter, followed by the application of a hydrostatic pressure of 160 MPa. The green disks were sintered in air at 1300 °C for 6 h. The measured densities were about 90% of theoretical ones, which enabled the measurements of bulk oxygen permeation rate. The chemical composition of the final product was confirmed by the inductively coupled plasma (ICP) spectroscopy and thermogravimetric measurements under hydrogen/nitrogen mixed gases.

Electrical Properties. Electrical conductivity of the PLNCG specimen was measured by a conventional DC 4-probes method in air using Pt electrode. The sintered disk was cut into a rectangular shape with the size of 1 mm × 5 mm × 15 mm, and four electrodes were fabricated with Pt paste. After firing at 1000 °C, the electrical conductivity was measured from 62 °C to 905 °C in air. Oxygen partial pressure (P_{O_2}) dependence of the electrical conductivity was measured by using H_2-H_2O, $CO-CO_2$, and N_2-O_2 gas mixtures and the P_{O_2} was monitored by using the oxygen sensor which was set close to the sample.

Oxygen Permeation Properties. Powders of the surface catalysts, $La_{0.6}Sr_{0.4}CoO_3$ and $La_{0.1}Sr_{0.9}Co_{0.9}Fe_{0.1}O_3$, were prepared by a similar solid-state reaction process. The appropriate amounts of cobalt acetate and nitrates of the other constituent cations were dissolved into distilled water. The $La_{0.6}Sr_{0.4}CoO_3$ and $La_{0.1}Sr_{0.9}Co_{0.9}Fe_{0.1}O_3$ powders obtained by drying the solution were fired at 1200 °C and 1100 °C, respectively, for 6 h. The resultant powders were ground and confirmed to be the single phase by a Rigaku X-ray powder diffractometer. The thickness of the sintered membrane was adjusted to be 0.5 mm by grinding with a diamond grinding machine. The oxygen permeation rate from air to He was measured by using the equipment described in ref 17. Dry air and He gas were supplied to each side of the specimen at a flow rate of 50 mL·min^{-1}. Oxygen permeation flux from air to He was measured in the temperature range of 600−1000 °C by a gas chromatograph (Shimadzu, GC-14A) equipped with the molecular sieves 5 Å column. There was no permeation through cracks and pores of the PLNCG specimen, and this was confirmed by monitoring the N_2 gas.

Neutron Diffraction Measurements and Data Analysis. We collected neutron powder diffraction data in air in the temperature range 27−1015.6 °C with a homemade furnace[30] and an angle dispersive-type neutron powder diffractometer, HERMES,[31] of the Institute for Materials Research (IMR), Tohoku University, installed in the JRR-3M reactor at the Japan Atomic Energy Agency (JAEA), Tokai, Japan. Neutrons with a wavelength of 1.82646(6) Å were obtained by 331 reflection of the Ge monochromator and 12′ blank sample/22′ collimation. The sintered PLNCG material was mounted in the high-temperature furnace,[30] which was set on the sample table of the HERMES diffractometer.[31] The diffracted beam was detected by a 150 ^{3}He detector system with Cd blades and slits in the 2θ range 5−155° at intervals of 0.1°. The collected data were analyzed by the Rietveld method, the maximum-entropy method (MEM), and MEM-based pattern fitting (MPF) with computer programs RIETAN-FP[32] and PRIMA.[33] Peak shape was ap-

(15) Adler, S. B. *Chem. Rev.* **2004**, *104*, 4791–4843.
(16) Stevenson, J. W.; Armstrong, T. R.; Carneim, R. D.; Pederson, L. R.; Weber, W. J. *J. Electrochem. Soc.* **1996**, *143*, 2722–2729.
(17) Ishihara, T.; Tsuruta, Y.; Todaka, T.; Nishiguchi, H.; Takita, Y. *Solid State Ionics* **2002**, *152−153*, 709–714.
(18) Shao, Z.; Haile, S. *Nature* **2004**, *431*, 170–173.
(19) Trunec, M.; Cihlar, J.; Diethelm, S.; Van herle, J. *J. Am. Ceram. Soc.* **2006**, *89*, 955–959.
(20) Ishihara, T.; Nakashima, K.; Okada, S.; Enoki, M.; Matsumoto, H. *Solid State Ionics* **2008**, *179*, 1367–1371.
(21) Aguadero, A.; Alonso, J. A.; Escudero, M. J.; Daza, L. *Solid State Ionics* **2008**, *179*, 393–400.
(22) Yashima, M.; Enoki, M.; Wakita, T.; Ali, R.; Matsushita, Y.; Izumi, F.; Ishihara, T. *J. Am. Chem. Soc.* **2008**, *130*, 2762–2763.
(23) Yamada, A.; Suzuki, Y.; Saka, K.; Uehara, M.; Mori, D.; Kanno, R.; Kiguchi, T.; Mauvy, F.; Grenier, J.-C. *Adv. Mater.* **2008**, *21*, 4124–4128.
(24) Yashima, M. In *Perovskite Oxide for Solid Oxide Fuel Cells*; Ishihara, T., Ed.; Fuel Cells and Hydrogen Energy; Springer Verlag: New York, 2009; pp 117−145.
(25) Kovalevsky, A. V.; Kharton, V. V.; Yaremechenko, A. A.; Pivak, Y. V.; Tsipis, E. V.; Yakovlev, S. O.; Markov, A. A.; Naumovich, E. N.; Frade, J. R. *J. Electroceram.* **2007**, *18*, 205–218.
(26) Skinner, S. J.; Kilner, J. A. *Solid State Ionics* **2000**, *135*, 709–712.
(27) Minervini, L.; Grimes, R. W.; Kilner, J. A.; Sickafus, K. E. *J. Mater. Chem.* **2000**, *10*, 2349–2354.
(28) Bassat, J. M.; Odier, P.; Villesuzanne, A.; Marin, C.; Pouchard, M. *Solid State Ionics* **2004**, *167*, 341–347.
(29) Boem, E.; Bassat, J.-M.; Dordor, P.; Mauvy, F.; Grenier, J.-C.; Stevens, Ph. *Solid State Ionics* **2005**, *176*, 2717–2725.
(30) Yashima, M. *J. Am. Ceram. Soc.* **2002**, *85*, 2925–2930.
(31) Ohoyama, K.; Kanouchi, T.; Nemoto, K.; Ohashi, M.; Kajitani, T.; Yamaguchi, Y. *Jpn. J. Appl. Phys., Part 1* **1998**, *37*, 3319–3326.
(32) Izumi, F.; Momma, K. *Solid State Phenom.* **2007**, *130*, 15–20.

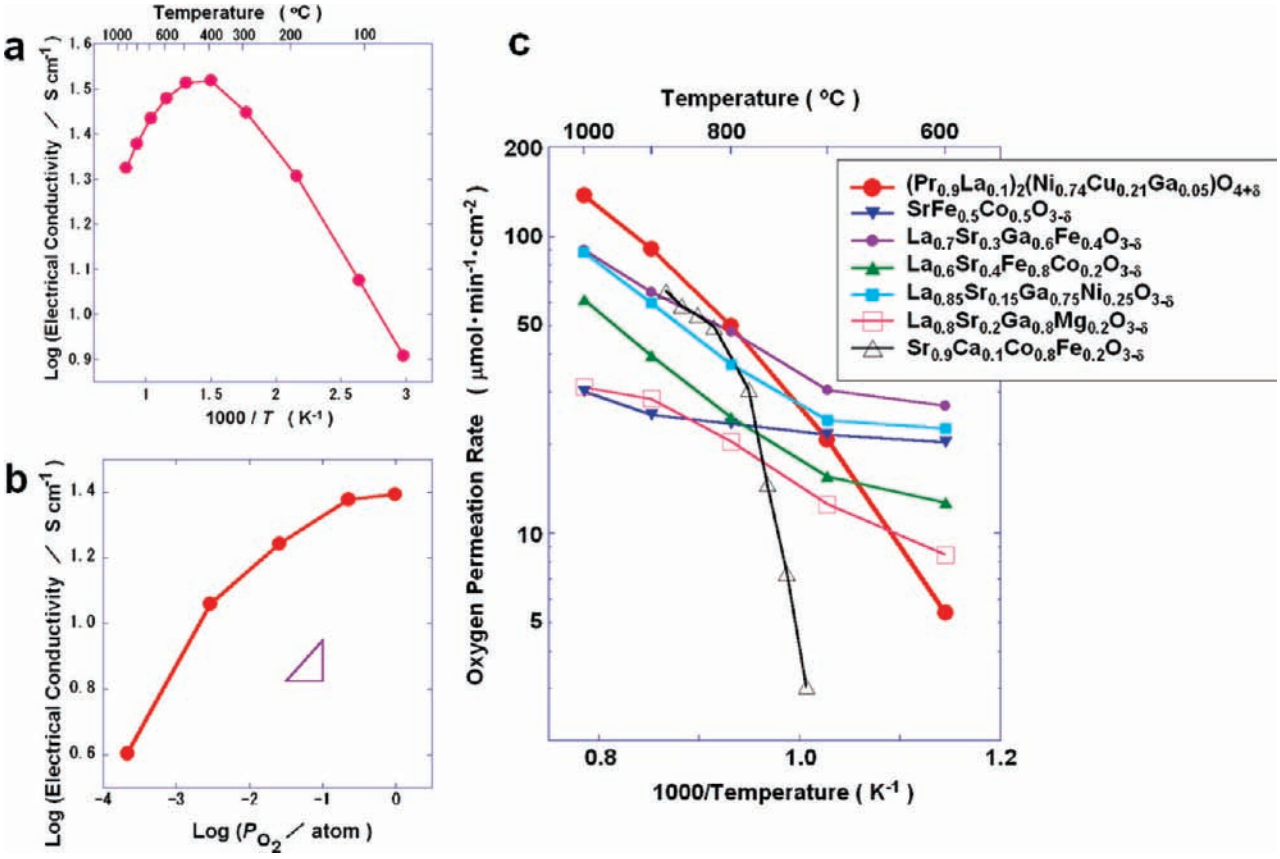

Figure 1. Electrical and oxygen permeation properties of $(Pr_{0.9}La_{0.1})_2(Ni_{0.74}Cu_{0.21}Ga_{0.05})O_{4+\delta}$ (PLNCG). (a) Temperature dependence of the total electrical conductivity of PLNCG in air. (b) Oxygen partial pressure P_{O_2} dependence of the total electrical conductivity of PLNCG at 800 °C, which indicates the p-type conduction. The increase of electrical conductivity with P_{O_2} strongly suggests that the major charge carrier in PLNCG is an electronic hole. The triangle shows the slope of 1/4 for the electrical conductivity against P_{O_2}, which is expected for the formation of electron hole. (c) Temperature dependence of the bulk oxygen permeation rate from air to He of PLNCG, which indicates quite high permeability. The data on selected $ABO_{3-\delta}$ perovskite-type mixed conductors[17] are also plotted for comparison. The rate is normalized for the thickness of 0.5 mm. $La_{0.1}Sr_{0.9}Co_{0.8}Fe_{0.2}O_{3-\delta}$ or $La_{0.6}Sr_{0.4}CoO_{3-\delta}$ catalyst (40 μm thickness) is coated, which enables the bulk permeation. Flows of (He 200 mL/min or CH_4:N_2 = 2:1 gas 50 mL/min) and (air 200 mL/min or 50 mL/min) are used.

proximated by split pseudo-Voigt function, and the background profile was approximated with a 12-parameter Legendre polynomial. The unit cell, zero point, background, profile shape, and crystal structural parameters were simultaneously refined. The coherent scattering lengths adopted for Rietveld refinements were 4.58 fm for Pr, 8.24 fm for La, 10.30 fm for Ni, 7.718 fm for Cu, 7.288 fm for Ga, and 5.803 fm for O. The 44 reflections were used for MEM calculations with a 32 × 32 × 128 pixel unit cell. The crystal structure and density distributions were visualized using the VESTA computer program.[34]

Synchrotron Diffraction Measurements and Data Analysis. Synchrotron X-ray powder diffraction analyses were performed using the multiple-detector system,[35] installed at the BL-4B$_2$ beamline of the Photon Factory operated by the High Energy Accelerator Research Organization (KEK), Japan. The experimental setup consisted of a bending magnet light source, a double-crystal Si(111) monochromator, a focusing cylindrical mirror, and a multiple detector system with Ge(111) analyzer crystals, Soller slits, and scintillation counters. A monochromatized 1.20641 Å X-ray beam was utilized. Powder diffraction data from the powdered PLNCG sample at 25 °C in air were collected in asymmetric flat-specimen reflection geometry with a fixed incident angle of 7.0°. Scanning parameters were set as follows: step interval, 0.004°; counting time, 3 s step^{-1}; diffraction angle (2θ), 8−120°. The crystal structure of the PLNCG sample was refined by the Rietveld method using RIETAN-FP.[32] As enhancement in asymmetric scan mode is not implemented in RIETAN-FP, the observed intensity data were modified by multiplying by the term $[1 + \{\sin\alpha/\sin(2\theta - \alpha)\}]/2$, where α is the fixed incident angle, in order to obtain data equivalent to those measured in symmetric scan mode. The peak shape was assumed to be a split Pearson VII-type function, and the cutoff value was set at 30 times the full-width at half-maximum (FWHM). The background was approximated with a 12-parameter Legendre polynomial. The 12 variables were refined simultaneously with the unit cell, zero-point, scale, profile shape, and crystal structural parameters. The electron-density distribution of PLNCG was investigated by the MEM using the 96 structure factors obtained by the Rietveld analysis. MEM calculations were carried out using the computer program PRIMA[33] with a 32 pixel × 32 pixel × 128 pixel unit cell.

Density Functional Theory Based Calculations. The generalized gradient approximation (GGA) electronic calculations were performed with Vienna *Ab initio* Simulation Package (VASP),[36] to examine the ground state and optimized crystal structure of tetragonal $Pr_{36}La_4Ni_{15}Cu_4GaO_{84}$ which is an approximated composition of the $(Pr_{0.9}La_{0.1})_2(Ni_{0.74}Cu_{0.21}Ga_{0.05})O_{4+\delta}$. The optimized structure of $Pr_{36}La_4Ni_{15}Cu_4GaO_{84}$ is shown in Figure 4d. The 5 × 2 × 1 supercell $Pr_{36}La_4Ni_{15}Cu_4GaO_{84}$ contains 20

(33) Izumi, F.; Dilanian, R. A. *Recent Res. Dev. Phys.* **2002**, *3*, 699–726.
(34) Momma, K.; Izumi, F. *J. Appl. Crystallogr.* **2008**, *41*, 653–658.
(35) Toraya, H.; Hibino, H.; Ohsumi, K. *J. Synchrotron Rad.* **1996**, *3*, 75–84.
(36) Kresse, G.; Joubert, D. *Phys. Rev. B* **1999**, *59*, 1758–1775.

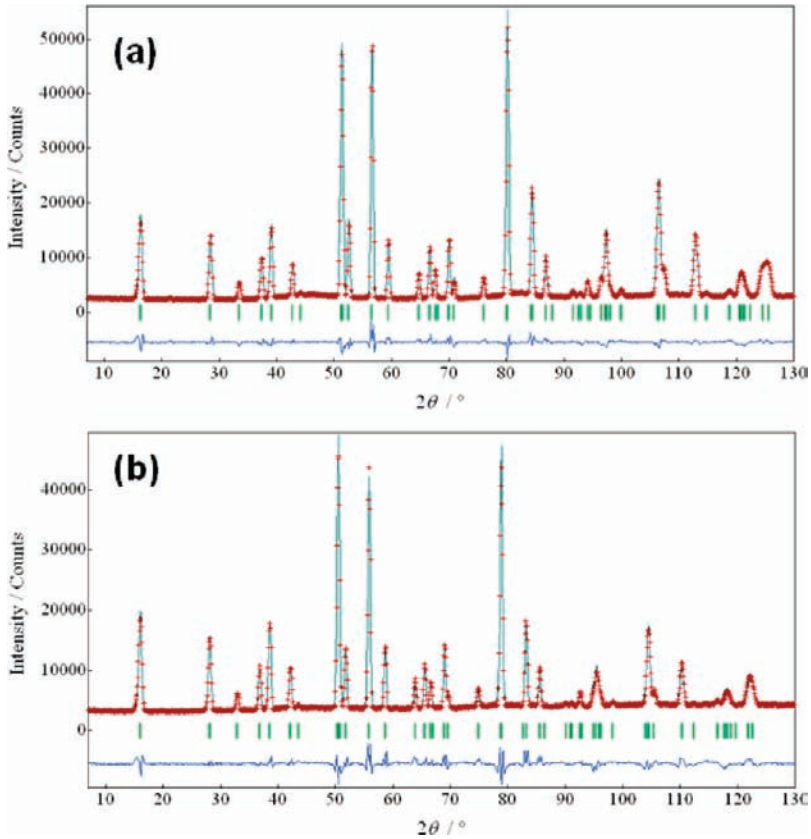

Figure 2. Rietveld fitting results for the neutron diffraction data of $(Pr_{0.9}La_{0.1})_2(Ni_{0.74}Cu_{0.21}Ga_{0.05})O_{4+\delta}$ measured at (a) 27 °C and (b) 1015.6 °C. The red plus symbols and the green line denote the observed and calculated intensities, respectively. Short verticals indicate the positions of possible Bragg reflections. The difference between the observed and calculated profiles is plotted at the bottom. The wavelength of the incident neutrons is 1.82646 Å. Rietveld fittings were performed by the tetragonal *I*4/*mmm* structured $(Pr_{0.9}La_{0.1})_2(Ni_{0.74}Cu_{0.21}Ga_{0.05})O_{4+\delta}$.

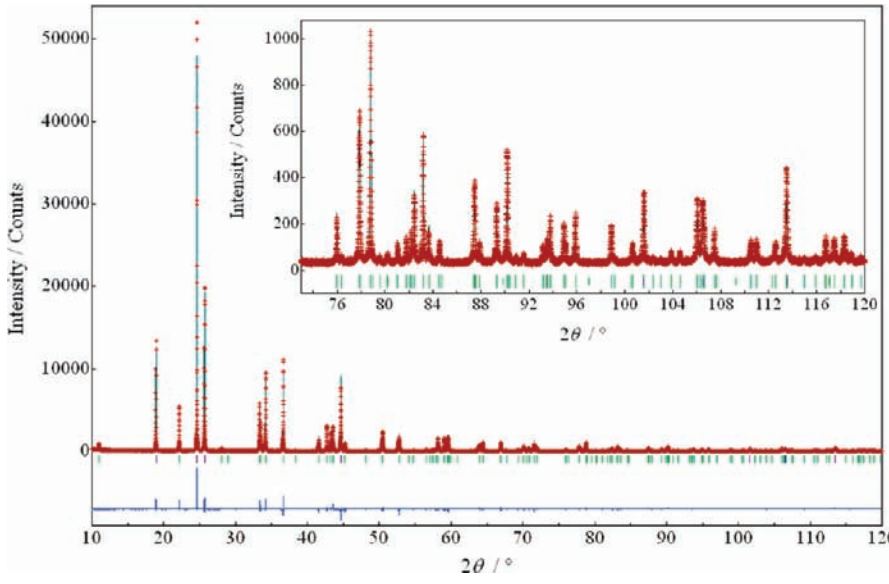

Figure 3. Rietveld fitting results for the high angular resolution ($\delta d/d = 0.04\%$) synchrotron X-ray diffraction data of $(Pr_{0.9}La_{0.1})_2(Ni_{0.74}Cu_{0.21}Ga_{0.05})O_{4+\delta}$ measured at 25 °C. The red plus symbols and the green line denote the observed and calculated intensities, respectively. Short verticals indicate the positions of possible Bragg reflections. The difference between the observed and calculated profiles is plotted at the bottom. The wavelength of the incident X-ray is 1.20641 Å. No splitting of reflections for the orthorhombic phase appeared, which indicates the tetragonal symmetry of $(Pr_{0.9}La_{0.1})_2(Ni_{0.74}Cu_{0.21}Ga_{0.05})O_{4+\delta}$.

$(Pr_{0.9}La_{0.1})_2(Ni_{0.75}Cu_{0.20}Ga_{0.05})O_{4.2}$ formula units. A plane-wave basis set with a cutoff of 400 eV was used. The Perdew−Burke−Ernzerhof (PBE) GGA was employed for the exchange and correlation functionals.[37] Atomic coordinates were optimized with the convergence condition of 0.02 eV/Å. The positions of all atoms were relaxed in the space group *P*1. Unit cell and initial positional parameters used in the optimization were referred from the Rietveld refinements in this study. Optimized crystal

Table 1. Refined Crystal Parameters[a] and Reliability Factors in Rietveld Analysis of Neutron Diffraction Data of $(Pr_{0.9}La_{0.1})_2(Ni_{0.74}Cu_{0.21}Ga_{0.05})O_{4+\delta}$ at 27 °C ($\delta = 0.21(4)$)

site and atoms	Wyckoff position	occupancy factor *g*	fractional coordinate *x*	*y*	*z*	atomic displacement parameter *U* (Å^2)
$Pr_{0.90}La_{0.10}$	4*e*	1.0	0	0	0.3586(2)	0.0162(8)
Ni	2*a*	0.74(2)	0	0	0	0.0100(8)
Cu	2*a*	0.21(2)	0	0	0	= *U*(Ni)
Ga	2*a*	0.05	0	0	0	= *U*(Ni)
O1	4*c*	1.0	1/2	0	0	0.0151(8)
O2	4*e*	0.965(6)	0	0	0.1749(3)	0.0581[b]
O3	16*n*	0.035(2)	0.56(2)	0	0.233(3)	= 2*U*(O1) = 0.0302

[a] Note: Tetragonal space group *I*4/*mmm*, Number of formula units of $(Pr_{0.9}La_{0.1})_2(Ni_{0.74}Cu_{0.21}Ga_{0.05})O_{4+\delta}$ in a unit cell: $Z = 2$. Unit cell parameters: $a = b = 3.8333(11)$ Å. $c = 12.554(4)$ Å, $\alpha = \beta = \gamma = 90°$. Unit cell volume: 184.47(10) Å^3. *g*: Occupancy. *x*, *y*, *z*: fractional coordinates. *U*: Isotropic atomic displacement parameters. [b] Equivalent isotropic atomic displacement parameters, Anisotropic atomic displacement parameters of O2 atom: $U_{11} = U_{22} = 0.0826(15)$ Å^2, $U_{33} = 0.0092(15)$ Å^2, $U_{12} = U_{23} = U_{31} = 0$ Å^2. Reliability factors in the Rietveld analysis: $R_{wp} = 5.39\%$, $R_p = 3.88\%$, $R_e = 1.45\%$, $R_{wp}/R_e = 3.71$, $R_I = 1.19\%$, $R_F = 0.62\%$.

Table 2. Refined Crystal Parameters[a] and Reliability Factors in Rietveld Analysis of Synchrotron Diffraction Data of $(Pr_{0.9}La_{0.1})_2(Ni_{0.74}Cu_{0.21}Ga_{0.05})O_{4+\delta}$ at 25 °C ($\delta = 0.21(4)^b$)

site and atoms	Wyckoff position	occupancy factor *g*	fractional coordinate *x*	*y*	*z*	atomic displacement parameter *U* (Å^2)
$Pr_{0.90}La_{0.10}$	4*e*	1.0	0	0	0.35981(3)	0.02850(13)
Ni	2*a*	0.74(2)	0	0	0	0.0239(8)
Cu	2*a*	0.21(2)	0	0	0	= *U*(Ni)
Ga	2*a*	0.05	0	0	0	= *U*(Ni)
O1	4*c*	1.0	1/2	0	0	0.0444(12)
O2	4*e*	0.965[b]	0	0	0.1720(4)	0.152[c]
O3	16*n*	0.035[b]	0.56[b]	0	0.233[b]	= 2*U*(O1) = 0.0888

[a] Note: Tetragonal space group *I*4/*mmm*. Number of formula units of $(Pr_{0.9}La_{0.1})_2(Ni_{0.74}Cu_{0.21}Ga_{0.05})O_{4+\delta}$ in a unit cell: $Z = 2$. Unit cell parameters: $a = b = 3.83797(1)$ Å, $c = 12.55404(3)$ Å; $\alpha = \beta = \gamma = 90°$. Unit cell volume: 184.9213(8) Å^3. *g*: Occupancy. [b] The δ, *g*(O2), *g*(O3), and positional parameters of O3 atom were fixed to those from neutron diffraction analysis. *x*, *y*, *z*: fractional coordinates, *U*: Isotropic atomic displacement parameters. [c] Equivalent isotropic atomic displacement parameters, anisotropic atomic displacement parameters of O2 atom: $U_{11} = U_{22} = 0.206(6)$ Å^2, $U_{33} = 0.214 * U_{11} = 0.044$ Å^2, $U_{12} = U_{23} = U_{31} = 0$ Å^2. Reliability factors in the Rietveld analysis: $R_{wp} = 13.47\%$, $R_p = 10.54\%$, $R_e = 8.72\%$, $R_{wp}/R_e = 1.544$, $R_I = 6.05\%$, $R_F = 3.72\%$.

structures and valence electron density distributions were drawn with a computer program VESTA.[34]

Results and Discussion

The PLNCG exhibited a significant level of electronic conductivity (Figure 1a,b). The total electrical conductivity of PLNCG increased with increasing temperature between 62 °C and 394 °C, which indicates the semiconducting behavior. The electrical conductivity of PLNCG decreased with temperature above 490 °C, indicating the metallic nature. The total conductivity increased with an increase of oxygen partial pressure as shown in Figure 1b, which indicates the formation of electron−hole. Figure 1c shows the temperature dependence of bulk oxygen permeation rate of the K_2NiF_4-type PLNCG and some $ABO_{3-\delta}$ perovskite-type MIECs. The permeation rate of PLNCG increased with an increase of temperature. It should be noted that the oxygen permeation rate of PLNCG is quite high (137 μmol cm^{-2} min^{-1} at 1000 °C) in comparison with the conventional $ABO_{3-\delta}$ perovskite-type MIECs in the literature.[17] Thus, the PLNCG can be utilized as materials for oxygen separation membranes and cathodes of SOFCs.

Table 3. Refined Crystal Parameters[a] and Reliability Factors in Rietveld Analysis of Neutron Diffraction Data of $(Pr_{0.9}La_{0.1})_2(Ni_{0.74}Cu_{0.21}Ga_{0.05})O_{4+\delta}$ at 1015.6 °C ($\delta = 0.15(2)$)

site and atoms	Wyckoff position	occupancy factor *g*	fractional coordinate *x*	*y*	*z*	atomic displacement parameter *U* (Å^2)
$Pr_{0.90}La_{0.10}$	4*e*	1.0	0	0	0.3573(4)	0.0347(14)
Ni	2*a*	0.74(4)	0	0	0	0.0192(14)
Cu	2*a*	0.21(4)	0	0	0	= *U*(Ni)
Ga	2*a*	0.05	0	0	0	= *U*(Ni)
O1	4*c*	1.0	1/2	0	0	0.0315(14)
O2	4*e*	1.0	0	0	0.1752(4)	0.0840[b]
O3	16*n*	0.019(3)	0.666(19)	0	0.223(9)	= 2*U*(O1) = 0.0630

[a] Note: Tetragonal space group *I*4/*mmm*. Number of formula units of $(Pr_{0.9}La_{0.1})_2(Ni_{0.74}Cu_{0.21}Ga_{0.05})O_{4+\delta}$ in a unit cell: $Z = 2$. Unit cell parameters: $a = b = 3.875(3)$ Å, $c = 12.738(9)$ Å, $\alpha = \beta = \gamma = 90°$. Unit cell volume: 191.2(2) Å^3. *g*: Occupancy. *x*, *y*, *z*: fractional coordinates. *U*: Isotropic atomic displacement parameters. [b] Equivalent isotropic atomic displacement parameters, Anisotropic atomic displacement parameters of O2 atom: $U_{11} = U_{22} = 0.115(3)$ Å^2, $U_{33} = 0.021(3)$ Å^2, $U_{12} = U_{23} = U_{31} = 0$ Å^2. Reliability factors in the Rietveld analysis: $R_{wp} = 6.48\%$, $R_p = 4.59\%$, $R_e = 1.35\%$, $R_{wp}/R_e = 4.78$, $R_I = 2.18\%$, $R_F = 1.21\%$.

Neutron diffraction profiles include useful information on oxygen, because the scattering ability of the oxygen nucleus (amplitude of coherent scattering length) is relatively large and independent of diffraction angle. This nature enables detailed analysis of the small amount of interstitial oxygen atoms, nuclear density distribution, thermal motion and diffusional pathway of oxygen atoms. Furthermore the neutron diffraction is a powerful method to collect quality data at high temperatures.[22,30,38,39] On the other hand, the high-angular-resolution synchrotron diffraction data give the information on the crystal symmetry and chemical bonding.[40]

Neutron and synchrotron powder diffraction patterns indicated that the PLNCG material has a K_2NiF_4-type structure with tetragonal *I*4/*mmm* space group from 25 °C to 1015.6 °C in air (Figures 2 and 3, Tables 1, 2 and 3, Supporting Information, Figure S1). High-angular-resolution synchrotron X-ray diffraction profiles at 25 °C did not exhibit any splitting due to the orthorhombic symmetry, which indicates the tetragonal symmetry (Figure 3). Rietveld fitting by the tetragonal *I*4/*mmm* K_2NiF_4-type structure was satisfactory with accurately refined atomic positions as well as atomic displacement parameters for all atoms under the classical harmonic oscillation model (Figures 2 and 3, Tables 1, 2, and 3, and Supporting Information [Figure S1 and cif files]). For example, the reliability factors for the analysis of neutron data of PLNCG at 27 °C were $R_{wp} = 5.39\%$ and $R_F = 0.62\%$, and those at 1015.6 °C were $R_{wp} = 6.48\%$ and $R_F = 1.21\%$. The reliability factors for the analysis of synchrotron data of PLNCG at 25 °C were $R_{wp} = 13.47\%$ and $R_F = 3.72\%$. The crystal structure of PLNCG consists of (Ni,Cu,Ga)O_6 octahedron and (Pr,La)-O layers. In the (Pr,La)-O layer, interstitial O3 atoms existed at a 16*n* site, i.e., (*x*, 0, *z*) where $x = 0.56(2)$ and $z = 0.233(3)$ at 27 °C, which leads to the excess oxygen δ in $(Pr_{0.9}La_{0.1})_2(Ni_{0.74}Cu_{0.21}Ga_{0.05})O_{4+\delta}$ ($\delta = 0.21(4)$ at 27 °C). The amount of excess oxygen was

(37) Perdew, J.; Burke, K.; Ernzerhof, M. *Phys. Rev. Lett.* **1996**, *77*, 3865–3868.
(38) Yashima, M. *Solid State Ionics* **2008**, *179*, 797–803.
(39) Yashima, M. *J. Ceram. Soc. Jpn.* **2009**, *117*, 1055–1059.
(40) Yashima, M.; Ogisu, K.; Domen, K. *Acta Crystallogr., Sect. B* **2008**, *64*, 291–298.

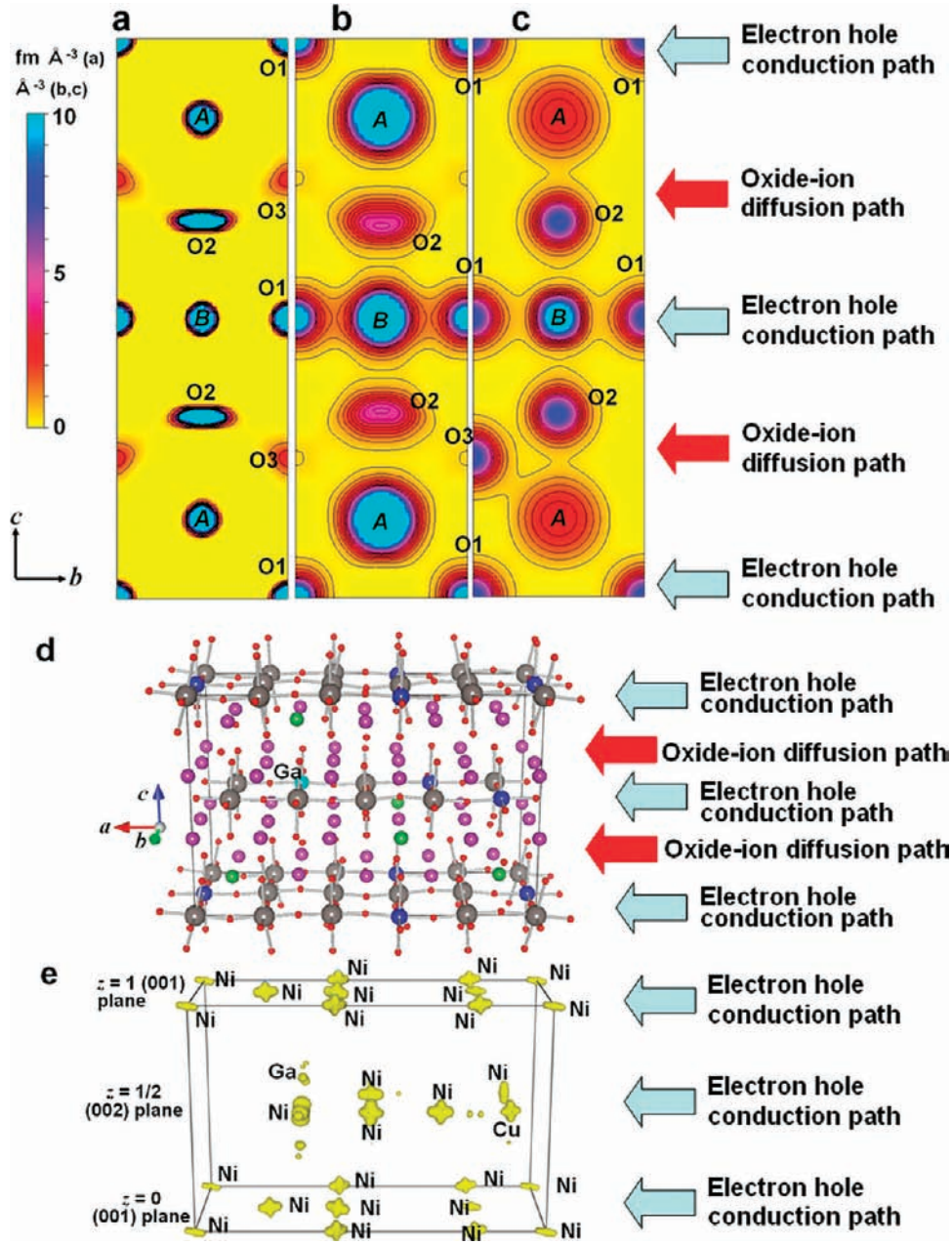

Figure 4. Structure, and nuclear and electron density distributions of $(Pr_{0.9}La_{0.1})_2(Ni_{0.74}Cu_{0.21}Ga_{0.05})O_{4+\delta}$ (PLNCG) at room temperature. (a) Nuclear density distribution on the *bc* plane at $x = 1/2$ of PLNCG, which was obtained by the combined technique of Rietveld, maximum-entropy method (MEM) and MEM-based pattern fitting (MPF) analyses of neutron powder diffraction data taken at 27 °C. Contour in the range 0−1 fm Å^{-3} (0.1 fm Å^{-3} per step). O3 is the interstitial oxygen atom. *A* and *B* are the (Pr,La) and (Ni,Cu,Ga) atoms, respectively. (b) Electron density distribution on the *bc* plane at $x = 1/2$ of PLNCG, which was obtained by the combined techniques of Rietveld, MEM, and MPF analyses of synchrotron X-ray powder diffraction data taken at 25 °C. Contour in the range from 0.4 to 5 Å^{-3} (0.5 Å^{-3} per step). (c) A corresponding valence electron density distribution of $Pr_{36}La_4Ni_{15}Cu_4GaO_{84}$, which was obtained by the density functional theory (DFT) calculations for the optimized structure depicted in Figure 4d. The optimized structure indicates the validity of interstitial O3 atom. (d) Optimized structure of $Pr_{36}La_4Ni_{15}Cu_4GaO_{84}$. Purple, green, gray, blue, light-blue, and red spheres are Pr, La, Ni, Cu, Ga, and O atoms, respectively. (e) Isosurface of highest occupied molecular orbitals (HOMO) of optimized $Pr_{36}La_4Ni_{15}Cu_4GaO_{84}$ at 0.054 Å^{-3}.

consistent with the TG (ThermoGravimetry) results measured under hydrogen/nitrogen gas flow. The excess oxygen in PLNCG ($\delta = 0.21$) is larger than that in the parent $Pr_2NiO_{4+\delta}$ ($\delta = 0.02-0.09$[25]), due to the doping of higher valence Ga^{3+} ion at the Ni^{2+} site. Both refined occupancy and TG measurements in air indicated that the amount of excess oxygen decreases with increasing temperature (Supporting Information, Figure S2). The refined unit cell parameters increased with temperature (see Supporting Information, Figure S3).

To evaluate the interstitial oxygen atoms, dynamic/static disorder of oxygen atoms and chemical bonding, MEM and MPF[32,33,38−40] were applied to estimate the neutron scattering length (nuclear) and electron density distributions. MEM is a model-free method used to calculate precise nuclear and electron densities in solids, including the information on the disorder, anharmonic vibrations and/or covalent bonds using experimentally obtained structure factors as an initial input. Successful MEM and MPF enhancements make it possible to evaluate not only the missing and heavily overlapped reflections but also any type of complicated electron or nuclear density distribution, which is hard to describe with a classical structure model. In MEM, any type of complicated electron or nuclear distribution

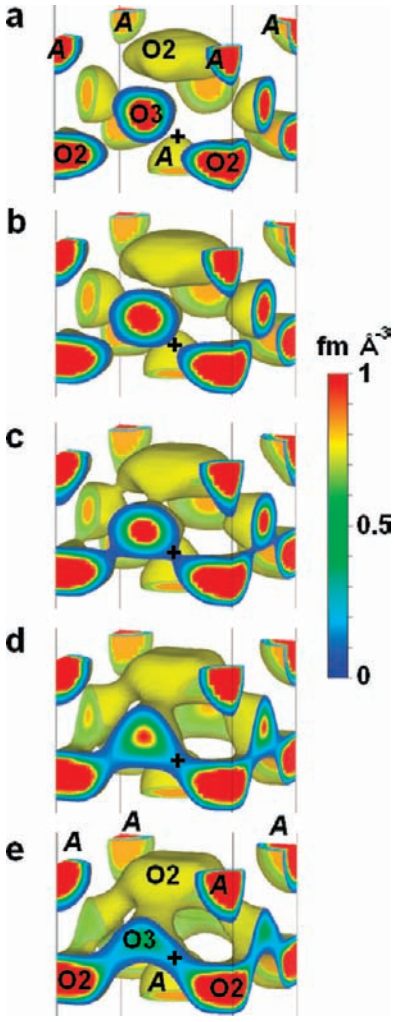

Figure 5. Equinuclear density surface at 0.05 fm Å^{-3} and nuclear density distribution on the (100) planes of $(Pr_{0.9}La_{0.1})_2(Ni_{0.74}Cu_{0.21}Ga_{0.05})O_{4+\delta}$ (PLNCG) at different temperatures, which indicates the diffusional pathway of oxide ions in the crystal lattice of PLNCG. These figures were obtained by the maximum-entropy method (MEM), MEM-based pattern fitting (MPF) and Rietveld analysis of neutron powder diffraction data of PLNCG measured *in situ* at 27 °C (a), 395.4 °C (b), 606.6 °C (c), 812.8 °C (d), and 1015.6 °C (e). The color scale denotes the values of nuclear density on the (100) planes of PLNCG. *A* denotes a (Pr,La) atom. The oxide ions diffuse through the oxygen O2−O3−O2 atomic sites. The cross (+) shows the bottleneck for the diffusional pathway between the oxygen O2 and O3 sites. The nuclear density at the bottleneck increases with an increase of temperature (see Figure 6a).

is allowed as long as it satisfies the symmetry requirements. The validity of such methodology has been well established for various materials.[38−40]

The interstitial O3 site was confirmed also in the nuclear and electron density maps obtained by the combined technique of Rietveld, MEM, and MPF analyses (Figure 4a,b and Figure 5). We optimized the crystal structure based on the density functional theory (DFT) using a supercell of $5 \times 2 \times 1$ (Figure 4d), which also indicates the validity of the interstitial oxygen site. The valence electron density map from DFT calculations (Figure 4c) is consistent with the experimental nuclear and electron densities (Figure 4a,b). Theoretical valence electron density map (Figure 4c) also confirms the interstitial O3 atom. The nuclear density at the O3 site decreased with increasing temperature (Figure 5), which is consistent with the decrease in occupancy factor at the O3 site and in the $4+\delta$ value in $(Pr_{0.9}La_{0.1})_2(Ni_{0.74}Cu_{0.21}Ga_{0.05})O_{4+\delta}$ (see Supporting Information Figure S2).

MEM electron and DFT valence electron density maps in b and c of Figure 4 include the information on chemical bonding in PLNCG. The covalent bonds between the (Ni,Cu,Ga) and O1 atoms are observed on the *ab* planes at $z = 0$ and 1/2 (*B*-O1 in b and c of Figure 4), while the (Pr,La) atoms are more ionic (*A* in parts b and c of Figure 4). The (Ni,Cu,Ga)-O1 covalent bond is formed by the overlap of Ni 3d, Cu 3d, and O1 2p orbitals (Supporting Information, Figure S4). The *B*-O1 covalent bonds form a two-dimensional network on the *ab* planes at $z = 0$ and 1/2. Figure 4e shows the equidensity surface of highest occupied molecular orbitals (HOMO) in PLNCG, which was obtained by the DFT calculations. As described before (Figure 1b), the electronic conduction occurs via electron−hole. The HOMO density map indicates the conduction path of electron−hole in PLNCG, which also forms a two-dimensional network on the *ab* planes at $z = 0$ and 1/2 (Figure 4).

Important information is included in the anisotropic atomic displacement parameters for oxygen, which determines the overall anisotropy of the thermal vibration by the shape of the ellipsoid. The oxygen atom at the apical O2 site (4*e*; (0, 0, *z*); $z = 0.1752(4)$ at 1015.6 °C) exhibited highly anisotropic thermal motion ($U_{11} = U_{22} = 0.115(3)$ Å^2, and $U_{33} = 0.021(3)$ Å^2), which leads to the migration of oxide ions to the nearest-neighbor interstitial O3 positions. The corresponding highly anisotropic distribution of apical O2 atoms was observed in both nuclear and electron density maps in Figure 4a,b and Figure 5. The DFT valence electron density map (Figure 4c) did not exhibit such an anisotropic feature, because this map was calculated for the ground state at 0 K without the thermal vibrations.

The striking feature is the oxygen diffusion pathway through the anisotropic O2 and interstitial O3 sites in PLNCG, which form the two-dimensional network of oxygen diffusion pathways. Figure 5 indicates that the interstitial O3 and anisotropic thermal motion of O2 play essential roles in the oxygen diffusion process. More excess oxygen in PLNCG ($\delta = 0.21$) compared with oxygen in the parent $Pr_2NiO_{4+\delta}$ ($\delta = 0.02-0.09$[25]) would be a factor of its high oxygen permeability, because oxygen diffusion occurs by the interstitial oxygen O3 site. Therefore, doping the higher-valence Ga^{3+} cation at the Ni^{2+} site improves the oxygen permeability, which is consistent with the previous work.[20]

The diffusional pathway was more prominent at higher temperatures (Figure 5). The minimum nuclear density on the diffusional pathway in PLNCG increased with an increase of temperature (+ in Figure 5 and in Figure 6a), which is consistent with the increase of oxygen permeation rate with temperature (Figure 1c). It is interesting that the minimum nuclear density at the bottleneck increases with temperature, although the amount of the interstitial O3 atom decreases.

Figures 1c and 6a show Arrhenius plots of the oxygen permeation rate and the minimum nuclear density on the O2−O3 diffusional pathway in PLNCG, respectively. The activation energy for the oxygen probability density at the bottleneck decreased with an increase of temperature as well as that for the bulk oxygen permeation rate. The activation energy of PLNCG at 950 °C is low (51 kJ/mol), which would be responsible for the high oxygen permeation rate. The activation energy for oxygen permeation rate of the present PLNCG is in

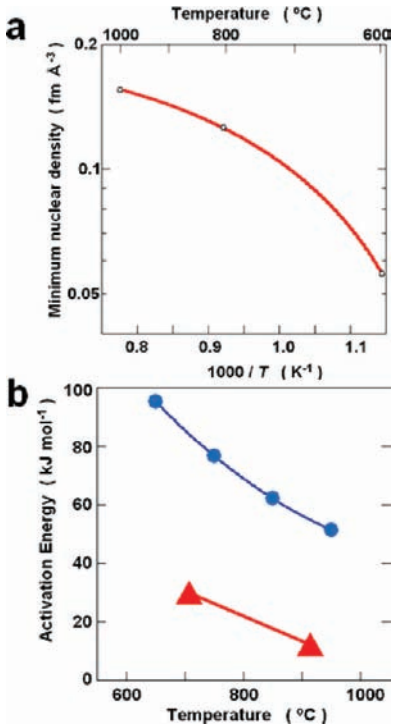

Figure 6. Activation energies for bulk oxygen movements in $(Pr_{0.9}La_{0.1})_2(Ni_{0.74}Cu_{0.21}Ga_{0.05})O_{4+\delta}$ (PLNCG), which demonstrates the correlation between its oxygen permeability and structure. (a) Arrhenius plot of minimum nuclear density on the O2−O3−O2 diffusional pathway of oxide ions in PLNCG. The density values at the cross (+) in Figure 5 were plotted in Figure 6a. (b) Temperature dependence of activation energies. Circles denote the activation energy estimated from the Arrhenius plot of oxygen permeation rate in Figure 1c. Triangles denote the activation energy estimated from the Arrhenius plot of minimum nuclear density on the O2−O3−O2 diffusional pathway of oxide ions in Figure 6a. The activation energy was obtained by drawing a straight line between two adjacent data points and taking the slope. The error bar of activation energy through this procedure was estimated to be less than 1.5%.

the range 51−95 kJ/mol, while those of conventional $ABO_{3-\delta}$ perovskite-type MIECs such as $La_{1-x}Sr_xGa_{1-y}Fe_yO_{3-\delta}$ and $La_{1-x}Ca_xCo_{1-y}Fe_yO_{3-\delta}$ are in the range 41−144 kJ/mol.[19] Doping of Ga and Cu atoms into the $Pr_2NiO_{4+\delta}$ host (97 kJ/mol in $Pr_2NiO_{4+\delta}$ around 825 °C)[25] is effective to decrease the activation energy for the oxygen permeation rate (62 kJ/mol in the present PLNCG around 850 °C). Higher symmetry of the tetragonal *I*4/*mmm* PLNCG (Figures 2 and 3 and Figure S1 in the Supporting Information) is a factor of the lower activation energy for oxygen permeation rate, comparing with the lower symmetry of the orthorhombic *Bmab* $Pr_2NiO_{4+\delta}$. It was reported that the oxygen permeation rate of the parent compound $Pr_2NiO_{4+\delta}$ decreased above 850 °C due to the decomposition into $Pr_4Ni_3O_{10-\delta}$ and Pr_2O_3.[25] On the contrary, the permeation rate of this PLNCG increased with an increase of temperature even at higher temperatures, because no such phase decomposition occurred. It is noteworthy that the activation energy from the nuclear density at the bottleneck of oxygen diffusion at 900 °C is extremely low (12 kJ/mol). This indicates possible higher bulk oxygen permeation rates in quality single crystals and epitaxial thin films.

Conclusions

In conclusion, we investigated the oxygen permeability and electrical properties and detailed crystal structure of K_2NiF_4-type $(Pr_{0.9}La_{0.1})_2(Ni_{0.74}Cu_{0.21}Ga_{0.05})O_{4+\delta}$ (PLNCG). We applied Rietveld, MEM, and MEM-based pattern fitting to neutron and synchrotron diffraction data of PLNCG measured *in situ* from 25 °C to 1015.6 °C and successfully visualized the two-dimensional curved oxygen diffusion path through the anisotropic O2 and interstitial O3 sites in PLNCG. It was confirmed that the structure of PLNCG consists of the oxygen diffusive O2−O3 layer and electron−hole conductive (Ni,Cu,Ga)-O1 layers (Figure 4). Beyond PLNCG, this would be important knowledge for the design of MIECs. This work has demonstrated that PLNCG exhibits a high oxygen permeation rate (137 μmol cm^{-2} min^{-1} at 1000 °C) and that the activation energy for oxygen permeation rate is low (51 kJ/mol around 950 °C). The activation energy from the MEM oxygen probability density at the bottleneck was found to be lower (12 kJ/mol around 900 °C), which indicates possible higher bulk oxygen permeation rates in quality single crystals and epitaxial thin films. Beyond PLNCG this is, to our knowledge, the first estimate of activation energy from the MEM probability density in MIECs. This procedure can be applied to various ionic and mixed conductors in order to shed light on the ion dynamics.

Acknowledgment. We thank Prof. K. Ohoyama, Prof. T. Ida, and Mr. K. Nemoto for their support on the neutron and synchrotron diffraction experiments. We also acknowledge Dr. T. Wakita for the arrangement of ICP measurements. A part of this work was financially supported by the Ministry of Education, Culture, Sports, Science and Technology of Japan, through a Grant-in-Aid for Scientific Research (B) No. 21360318. Correspondence and requests should be addressed to M.Y.

Supporting Information Available: Crystallographic data; Rietveld fitting results of neutron data, temperature dependence of amount of oxygen $4+\delta$, unit cell parameters in $(Pr_{0.9}La_{0.1})_2(Ni_{0.74}Cu_{0.21}Ga_{0.05})O_{4+\delta}$, and electronic density of states. This material is available free of charge via the Internet at http://pubs.acs.org.

JA909820H